Inorg. Chem. **2003**, *42*, 7067–7076

Heptanuclear and Decanuclear Manganese Complexes with the Anion of 2-Hydroxymethylpyridine

Nicholas C. Harden,[†] Milissa A. Bolcar,[‡] Wolfgang Wernsdorfer,[#] Khalil A. Abboud,[†] William E. Streib,[‡,§] and George Christou*[,†,‡]

Department of Chemistry, University of Florida, Gainesville, Florida 32611-7200, Department of Chemistry and Molecular Structure Center, Indiana University, Bloomington, Indiana 47405-4001, and Laboratoire Louis Néel-CNRS, BP166, 25 Avenue des Martyrs, 38042 Grenoble, Cedex 9, France

Received July 28, 2003

The synthesis and magnetic properties are reported of two new clusters $[Mn_{10}O_4(OH)_2(O_2CMe)_8(hmp)_8](ClO_4)_4$ (**1**) and $[Mn_7(OH)_3(hmp)_9Cl_3](Cl)(ClO_4)$ (**2**). Complex **1** was prepared by treatment of $[Mn_3O(O_2CMe)_6(py)_3](ClO_4)$ with 2-(hydroxymethyl)pyridine (hmpH) in CH_2Cl_2, whereas **2** was obtained from the reaction of $MnCl_2{\cdot}4H_2O$, hmpH, and $NBu^n{}_4MnO_4$ in MeCN followed by recrystallization in the presence of $NBu^n{}_4ClO_4$. Complex $\mathbf{1}{\cdot}2py{\cdot}10CH_2Cl_2{\cdot}2H_2O$ crystallizes in the triclinic space group $P\bar{1}$. The cation consists of 10 Mn^{III} ions, 8 μ_3-O^{2-} ions, 2 μ_3-OH^- ions, 8 bridging acetates, and 8 bridging and chelating hmp^- ligands. The hmp^- ligands bridge through their O atoms in two ways: two with μ_3-O atoms and six with μ_2-O atoms. Complex $\mathbf{2}{\cdot}3CH_2Cl_2{\cdot}H_2O$ crystallizes in the triclinic space group $P\bar{1}$. The cation consists of four Mn^{II} and three Mn^{III} ions, arranged as a Mn_6 hexagon of alternating Mn^{II} and Mn^{III} ions surrounding a central Mn^{II} ion. The remaining ligation is by three μ_3-OH^- ions, three terminal chloride ions, and nine bridging and chelating hmp^- ligands. Six hmp^- ligands contain μ_2-O atoms and three contain μ_3-O atoms. The Cl^- anion is hydrogen-bonded to the three μ_3-OH^- ions. Variable-temperature direct current (dc) magnetic susceptibility data were collected for complex **1** in the 5.00–300 K range in a 5 kG applied field. The $\chi_M T$ value gradually decreases from 17.87 $cm^3\ mol^{-1}$ K at 300 K to 1.14 $cm^3\ mol^{-1}$ K at 5.00 K, indicating an $S = 0$ ground state. The ground-state spin of complex **2** was established by magnetization measurements in the 0.5–3.0 T and 1.80–4.00 K ranges. Fitting of the data by matrix diagonalization, incorporating only axial anisotropy ($D\hat{S}_z{}^2$), gave equally good fits with $S = 10$, $g = 2.13$, $D = -0.14\ cm^{-1}$ and $S = 11$, $g = 1.94$, $D = -0.11\ cm^{-1}$. Magnetization versus dc field scans down to 0.04 K reveal no hysteresis attributable to single-molecule magnetism behavior, only weak intermolecular interactions.

Introduction

A wide variety of polynuclear Mn clusters have been synthesized to date with the metal in the oxidation state range of II−IV, including clusters with mixed-valency. These complexes usually contain carboxylate ligands, and they are usually molecular but are sometimes polymeric.[1] Molecular species with metal nuclearities up to 30 have been reported to date.[2,3] One of our interests in these molecules is the often large ground-state spin (S) that they possess and the resulting possibility that such molecules might function as single-molecule magnets (SMMs).[4] A SMM possesses a significant

* Author to whom correspondence should be addressed. E-mail: christou@chem.ufl.edu.
† University of Florida.
‡ Indiana University.
# Laboratoire Louis Néel.
§ Deceased.

(1) Tasiopoulos, A. J.; Harden, N. C.; Abboud, K. A.; Christou, G. *Polyhedron* **2003**, *22*, 133.
(2) (a) Aromi, G.; Aubin, S. M. J.; Bolcar, M. A.; Christou, G.; Eppley, H. J.; Folting, K.; Gatteschi, D.; Hendrickson, D. N.; Huffman, J. C.; Squire, R. C.; Tsai, H.-L.; Wang, S.; Wemple, M. W. *Polyhedron* **1998**, *17*, 3005. (b) Chakov, N. E.; Abboud, K. A.; Zakharov, L. N.; Rheingold, A. L.; Hendrickson, D. N.; Christou, G. *Polyhedron* **2003**, *22*, 1759. (c) Brockman, J. T.; Abboud, K. A.; Hendrickson, D. N.; Christou, G. *Polyhedron* **2003**, *22*, 1765. (d) Soler, M.; Wernsdorfer, W.; Abboud, K. A.; Hendrickson, D. N.; Christou, G. *Polyhedron* **2003**, *22*, 1777. (e) Soler, M.; Wernsdorfer, W.; Sun, Z.; Ruiz, D.; Huffman, J. C.; Hendrickson, D. N.; Christou, G. *Polyhedron* **2003**, *22*, 1783.
(3) Soler, M.; Rumberger, E.; Folting, K.; Hendrickson, D. N.; Christou, G. *Polyhedron* **2001**, *20*, 1365.
(4) Christou, G.; Gatteschi, D.; Hendrickson, D. N.; Sessoli, R. *MRS Bull.* **2000**, *25*, 66.

10.1021/ic0348906 CCC: $25.00
Published on Web 10/04/2003

energy barrier to relaxation of its magnetization vector, which arises from the combination of a large ground-state spin and a significant magnetoanisotropy of the Ising (easy-axis) type, as reflected by a negative axial zero-field splitting parameter, D. The upper limit of this energy barrier is given by $S^2|D|$ or $(S^2 - {}^1/_4)|D|$ for integer or half-integer spins, respectively.[4,5] For such reasons, there is a continuing need for new examples of molecular metal species that possess large ground-state S values.

The present work comprises the synthesis and study of both a Mn_7 hmp^- species and a Mn_{10} hmp^- species, where hmp^- is the anion of 2-(hydroxymethyl)pyridine and is a N,O bidentate chelate. The hmp^- chelate has already proven very useful to us in the past for the synthesis of a number of Mn clusters of varying nuclearities. Other than the Mn_7 and Mn_{10} species to be presented here, it has been used in Mn chemistry for the synthesis of Mn_4,[6] Mn_{12},[7] and Mn_{18}[8] clusters, which have turned out to be SMMs. The hmp^- group can be both a chelating and a bridging ligand, the latter by the alkoxide O atom. As a result, we have frequently found that it fosters the formation of high-nuclearity species.

In the present work, the use of hmp^- in two different reaction systems has led to two new high-nuclearity products, namely, a Mn^{III}_{10} cluster and a $Mn^{II}_4Mn^{III}_3$ mixed-valence cluster. We describe the syntheses, crystal structures, and magnetic properties of these two species. These products are useful new additions to the growing family of Mn clusters with the hmp^- chelate and should also prove useful for further synthesis, as recently demonstrated in the use of the Mn_{10} complex as a starting material for the synthesis of $[Mn_4(hmp)_6(NO_3)_4]$.[9]

Experimental Section

Synthesis. All manipulations were performed under aerobic conditions using materials as received. $[Mn_3O(O_2CMe)_6(py)_3](ClO_4)$ and $NBu^n_4MnO_4$ were prepared as described.[10]

$[Mn_{10}O_4(OH)_2(O_2CMe)_8(hmp)_8](ClO_4)_4$ (1). To a stirred, red-brown solution of $[Mn_3O(O_2CMe)_6(py)_3](ClO_4)$ (2.09 g, 2.40 mmol) in CH_2Cl_2 (75 mL) was added solid hmpH (0.40 g, 3.7 mmol). The mixture was stirred for another hour and then left undisturbed at ambient room temperature. After 7 days, the resulting red-brown crystals of **1**·2py·$10CH_2Cl_2$·$2H_2O$ were collected by filtration, washed with CH_2Cl_2, and dried in vacuo. The yield was 20%. Anal. Calcd for $[Mn_{10}O_4(OH)_2(O_2CMe)_8(hmp)_8](ClO_4)_4$·$^1/_2$py ($C_{66.5}H_{76.5}N_{8.5}O_{46}Cl_4Mn_{10}$): C, 32.98; H, 3.18; N, 4.92; Cl, 5.85. Found: C, 32.85; H, 3.29; N, 4.95; Cl, 5.76. Selected IR data (Nujol): 1601 (s), 1580 (s), 1400 (s), 1346 (s), 1285 (m), 1256 (w), 1235 (m), 1159 (m), 1092 (s), 1046 (s), 947 (w), 897 (w), 826 (w), 764 (m), 702 (m), 660 (m), 623 (s), 586 (m), 548 (m), 498 (w), 467 (w), 449 (w), 419 (w) cm^{-1}.

$[Mn_7(OH)_3(hmp)_9Cl_3](Cl)(ClO_4)$ (2). Solid hmpH (0.55 g, 5.0 mmol) was added to a stirred solution of $MnCl_2$·$4H_2O$ (0.30 g, 1.5 mmol) in MeCN (50 mL). To this was added solid $NBu^n_4MnO_4$ (0.36 g, 1.0 mmol) in small portions. The resulting dark brown solution was stirred for 1 h and rotoevaporated to dryness. The oily solid residue was redissolved in CH_2Cl_2 (15 mL), an excess of $NBu^n_4ClO_4$ (0.85 g, 2.5 mmol) was added, and the solution was filtered. Hexanes (5 mL) were added to the filtrate, and the solution was maintained undisturbed in a sealed flask. Brown crystals of **2**·$3CH_2Cl_2$·H_2O slowly grew over 2 weeks, and they were collected by filtration, washed with hexanes, and dried in air. The yield was 30%. Anal. Calcd for $[Mn_7(OH)_3(hmp)_9Cl_3](Cl)(ClO_4)$·$2CH_2Cl_2$·$H_2O$ ($C_{56}H_{63}N_9O_{17}Cl_9Mn_7$): C, 36.60; H, 3.46; N, 6.86. Found: C, 36.45; H, 3.46; N, 6.93. Selected IR data (KBr disk): 1606 (s), 1569 (w), 1482 (m), 1438 (s), 1363 (w), 1292 (m), 1224 (w), 1156 (m), 1121 (m), 1088 (s), 1078 (s), 1069 (s), 1045 (s), 1016 (m), 823 (w), 764 (s), 727 (m), 670 (m), 656 (m), 638 (m), 624 (m), 564 (s), 528 (m), 486 (w), 462 (w), 422 (w), 412 (w) cm^{-1}.

X-ray Crystallography and Solution of Structure. A suitable crystal of **1**·2py·$10CH_2Cl_2$·$2H_2O$ was attached to a glass fiber using silicone grease. It was then transferred to the goniostat of a locally modified Picker four-circle diffractometer at approximately −170 °C. Details of the diffractometry, low-temperature facilities, and computational procedures used by the Molecular Structure Center (Indiana University, Bloomington) are available elsewhere.[11]

A selective search of a limited hemisphere of reciprocal space revealed no symmetry among the observed intensities. The choice of space group $P\bar{1}$ was later proven correct by the successful solution of the structure. Following complete intensity data collection ($+h,+k,+l$), data processing produced a unique set of 8565 intensities and gave a residual of 0.058 for the averaging of the 2-fold redundant data. No correction was made for absorption.

The structure was solved using a combination of direct methods (MULTAN78) and Fourier techniques and refined by full-matrix least-squares analysis. The Mn_{10} cation lies on a crystallographic center of symmetry. In addition to the half cation, the asymmetric unit contains two ClO_4^- anions, one of which is reasonably well-ordered and one that has approximate 2-fold disorder. Also present are a well-ordered molecule of pyridine solvent, five disordered molecules of CH_2Cl_2 solvent that have occupancies ranging from 53% to 90%, and one additional peak, within hydrogen-bonding distance of an O atom on a ClO_4^- and a Cl atom on a CH_2Cl_2, which was modeled as a water molecule and which refined to an occupancy of 30%. Non-hydrogen atoms of the cation, the anions, and the pyridine molecule were refined with anisotropic displacement parameters; the remaining non-hydrogen atoms were refined with isotropic thermal parameters. Hydrogen atoms were included in fixed, calculated positions for the cation and the pyridine molecule, with thermal parameters fixed at one plus the isotropic thermal parameter of the carbon atom to which they are bonded. The final $R(F)$ was 0.084 for 798 total variables using all of the unique data. Data having $F < 3\sigma(F)$ were given zero weight. The

(5) (a) Sessoli, R.; Gatteschi, D.; Caneschi, A.; Novak, M. A. *Nature* **1993**, *365*, 141. (b) Sessoli, R.; Tsai, H.-L.; Schake, A. R.; Wang, S.; Vincent, J. B.; Folting, K.; Gatteschi, D.; Christou, G.; Hendrickson, D. N. *J. Am. Chem. Soc.* **1993**, *115*, 1804.

(6) Yoo, J.; Yamaguchi, A.; Nakano, M.; Krzystek, J.; Streib, W. E.; Brunel, L.-C.; Ishimoto, H.; Christou, G.; Hendrickson, D. N. *Inorg. Chem.* **2001**, *40*, 4604.

(7) Boskovic, C.; Brechin, E. K.; Streib, W. E.; Folting, K.; Bollinger, J. C.; Hendrickson, D. N.; Christou, G. *J. Am. Chem. Soc.* **2002**, *124*, 3725.

(8) (a) Sanudo, E. C.; Brechin, E. K.; Boskovic, C.; Wernsdorfer, W.; Yoo, J.; Yamaguchi, A.; Concolino, T. R.; Abboud, K. A.; Rheingold, A. L.; Ishimoto, H.; Hendrickson, D. N.; Christou, G. *Polyhedron* **2003**, *22*, 2267. (b) Brechin, E. K.; Boskovic, C.; Wernsdorfer, W.; Yoo, J.; Yamaguchi, A.; Sanudo, E. C.; Concolino, T. R.; Rheingold, A. L.; Ishimoto, H.; Hendrickson, D. N.; Christou, G. C. *J. Am. Chem. Soc.* **2002**, *124*, 9710.

(9) Yang, E.-C.; Harden, N. C.; Wernsdorfer, W.; Zakharov, L.; Brechin, E. K.; Rheingold, A. L.; Christou, G.; Hendrickson, D. N. *Polyhedron* **2003**, *22*, 1857.

(10) Vincent, J. B.; Chang, H.-R.; Folting, K.; Huffman, J. C.; Christou, G.; Hendrickson, D. N. *J. Am. Chem. Soc.* **1987**, *109*, 5703.

(11) Chisholm, M. H.; Folting, K.; Huffman, J. C.; Kirkpatrick, C. C. *Inorg. Chem.* **1984**, *23*, *1021*.

Table 1. Crystallographic Data for Complexes **1**·2py·10CH_2Cl_2·2H_2O and **2**·3CH_2Cl_2·H_2O

	complex	
	1	**2**
formula[a]	$C_{84}H_{108}N_{10}O_{48}Cl_{24}Mn_{10}$	$C_{57}H_{65}N_9O_{17}Cl_{11}Mn_7$
fw, g mol^{-1}	3426.05	1922.71
space group	$P\bar{1}$	$P\bar{1}$
a (Å)	15.772(4)	12.6352(6)
b (Å)	16.817(4)	14.6413(7)
c (Å)	14.237(3)	20.552(2)
α (deg)	113.57(1)	90.993(2)
β (deg)	108.80(1)	97.516(2)
γ (deg)	86.30(1)	91.883(2)
V (Å^3)	3267.43	3766.5(3)
Z	1	2
ρ_{calcd} (g cm^{-3})	1.740	1.695
T (°C)	−172	−80
λ (Å)[b]	0.710 73	0.710 73
μ (mm^{-1})	1.4727	1.594
R (R_w) (%)[c]	8.37 (8.26)	3.19 (9.06)

[a] Including solvate molecules. [b] Graphite monochromator. [c] $R = \sum||F_o| - |F_c||/\sum|F_o|$; wR2 $= [\sum[w(F_o^2 - F_c^2)^2]/\sum[w(F_o^2)^2]]^{1/2}$, where $w = 1/[\sigma^2(F_o^2) + (0.054p)^2]$ and $p = [\max(F_o^2,0) + 2F_c^2]/3$.

largest peak in the final difference Fourier map was 1.96 e Å^{-3} in a disordered solvent molecule, and the deepest hole was −1.02 e Å^{-3}.

Data for complex **2**·3CH_2Cl_2·H_2O were collected at −80 °C on a Siemens SMART PLATFORM equipped with a charge coupled device (CCD) area detector and a graphite monochromator utilizing Mo Kα radiation (μ = 0.710 73 Å). Cell parameters were refined using up to 8192 reflections. A full sphere of data (1850 frames) was collected using the ω-scan method (0.3° frame width). The first 50 frames were remeasured at the end of data collection to monitor instrument and crystal stability (maximum correction on I was <1%). Absorption corrections by integration were applied based on measured indexed crystal faces.

The structure was solved by the direct methods in SHELXTL5 and refined using full-matrix least-squares analysis.[12] The non-hydrogen atoms were refined anisotropically, whereas the hydrogen atoms were included in fixed, calculated positions with thermal parameters fixed at one plus the isotropic thermal parameter of the carbon atom to which they are bonded. The hydrogen atoms on the hydroxyl groups were located in a difference Fourier map and refined freely. The asymmetric unit contains the Mn_7 cation, a Cl^- ion, a ClO_4^- ion, three CH_2Cl_2 molecules, one of which has one of its Cl atoms disordered over two positions, and a water molecule whose H atoms were located in a difference Fourier map but were refined as riding on its O atom. A total of 932 parameters were refined in the final cycle of refinement on F^2 using 8409 reflections with $I > 2\sigma(I)$ to yield R1 and wR2 values of 3.19% and 9.06%, respectively.

Crystallographic data and structure refinement details for both complexes are listed in Table 1.

Other Measurements. Elemental analyses were performed by Atlantic Microlab, Inc. (Norcross, GA) and by the in-house facilities of the Chemistry Department, University of Florida. IR spectra were recorded as Nujol mulls with a Nicolet 520 FT-IR spectrometer or as KBr disks using a Nicolet Nexus 670 spectrophotometer. Variable-temperature, solid-state direct current (dc) magnetic susceptibility data down to 5.00 K were collected on a Quantum Design MPMS-XL SQUID magnetometer equipped with a 7 T dc magnet at the University of Florida. Diamagnetic corrections were applied to the observed paramagnetic susceptibilities using Pascal's constants. The dc measurements below 1.80 K were performed on single crystals using an array of micro-SQUIDS.[13]

Results and Discussion

Synthesis. The initial reaction explored was that between 1.5 equiv. of hmpH and $[Mn_3O(O_2CMe)_6(py)_3](ClO_4)$ in CH_2Cl_2. Such reactions between a triangular Mn_3 species containing three Mn^{III} ions and a chelating ligand have been previously explored by us for a wide variety of bidentate chelates, the first one employed being 2,2′-bipyridine (bpy), which resulted in formation of Mn_4 complexes with the $[Mn_4O_2]$ butterfly-like core.[14] For the reaction with hmpH, the product proved to be the Mn_{10} complex **1**. This species contains 10 Mn^{III} ions, and thus there was no change to the Mn oxidation level compared to the starting Mn_3 complex. However, the yield of **1** was small (20%), and it is likely, as with many other reactions in Mn^{III} chemistry, that the reaction solution contains a complicated mixture of several species in equilibrium, with factors such as relative solubility, lattice energies, crystallization kinetics, and others determining the identity of the isolated product. Along these lines, it is worth noting that the use of the benzoate analogue $[Mn_3O(O_2CPh)_6(py)_3](ClO_4)$[10] instead of $[Mn_3O(O_2CMe)_6(py)_3](ClO_4)$ in an otherwise identical reaction system did not lead to isolation of the benzoate analogue of **1** but instead led to crystallization of $[Mn_6O_2(O_2CPh)_{10}(py)_2(MeCN)_2]$ containing $4Mn^{II}$, $2Mn^{III}$, and no bound hmp^- groups. This and similar hexanuclear species differing in the identity of the bound neutral ligands have been previously observed and are common products at this oxidation level with benzoate groups.[15]

A few other Mn_{10} complexes have been reported in the literature. Addition of NMe_4OH to a solution of $MnCl_2$·$4H_2O$ and 2,2′-biphenol ($biphenH_2$) in EtOH resulted in the formation of $(NMe_4)_4[Mn_{10}(biphen)_4O_4Cl_{12}]$. The molecule has a $Mn^{II}_6Mn^{III}_4$ formulation, and single-crystal EPR data gave $S = 12$ and $D = -0.035$ cm^{-1}.[16] Another Mn_{10} cluster was formed from the dissolution of $[Mn_4O_2(O_2CPh)_6(MeCN)_2(pic)_2]$ (picH is picolinic acid) in $MeCONMe_2$ and CH_2Cl_2 in the presence of picH, which gave $[Mn_{10}O_8(O_2CPh)_6(pic)_8]$ possessing an $S = 0$ ground state.[17] The complex $(NEt_4)_2[Mn_{10}O_2Cl_8\{(OCH_2)_3CMe\}_6]$, obtained from the use of a triol chelate, contains $Mn^{II}_2Mn^{III}_8$ with an edge-sharing bi-octahedral Mn_{10} topology, but its ground-state spin value was not reported.[18] Finally, the $Mn^{III}_4Mn^{IV}_6$ complex $[Mn_{10}O_{14}\{N(CH_2CH_2NH_2)_3\}_6]$ is particularly relevant to the

(12) Sheldrick, G. M. *SHELXTL5*; Bruker-AXS: Madison, WI, 2000.

(13) Wernsdorfer, W. *Adv. Chem. Phys.* **2001**, *118*, 99.

(14) Vincent, J. B.; Christmas, C.; Chang, H.-R.; Li, Q.; Boyd, P. D. W.; Huffman, J. C.; Hendrickson, D. N.; Christou, G. *J. Am. Chem. Soc.* **1989**, *111*, 2086.

(15) (a) Schake, A. R.; Vincent, J. B.; Li, Q.; Boyd, P. D. W.; Folting, K.; Huffman, J. C.; Hendrickson, D. N.; Christou, G. *Inorg. Chem.* **1989**, *28*, 1915. (b) Blackman, A. G.; Huffman, J. C.; Lobkovsky, E. B.; Christou, G. *Polyhedron* **1992**, *11*, 251.

(16) (a) Goldberg, D. P.; Caneschi, A.; Lippard, S. J. *J. Am. Chem. Soc.* **1993**, *115*, 9299. (b) Goldberg, D. P.; Caneschi, A.; Delfs, C. D.; Sessoli, R.; Lippard, S. J. *J. Am. Chem. Soc.* **1995**, *117*, 5789.

(17) Eppley, H. J.; Aubin, S. M. J.; Streib, W. E.; Bollinger, J. C.; Hendrickson, D. N.; Christou, G. *Inorg. Chem.* **1997**, *36*, 109.

(18) Cavaluzzo, M.; Chen, Q.; Zubieta, J. *J. Chem. Soc., Chem. Commun.* **1993**, 131.

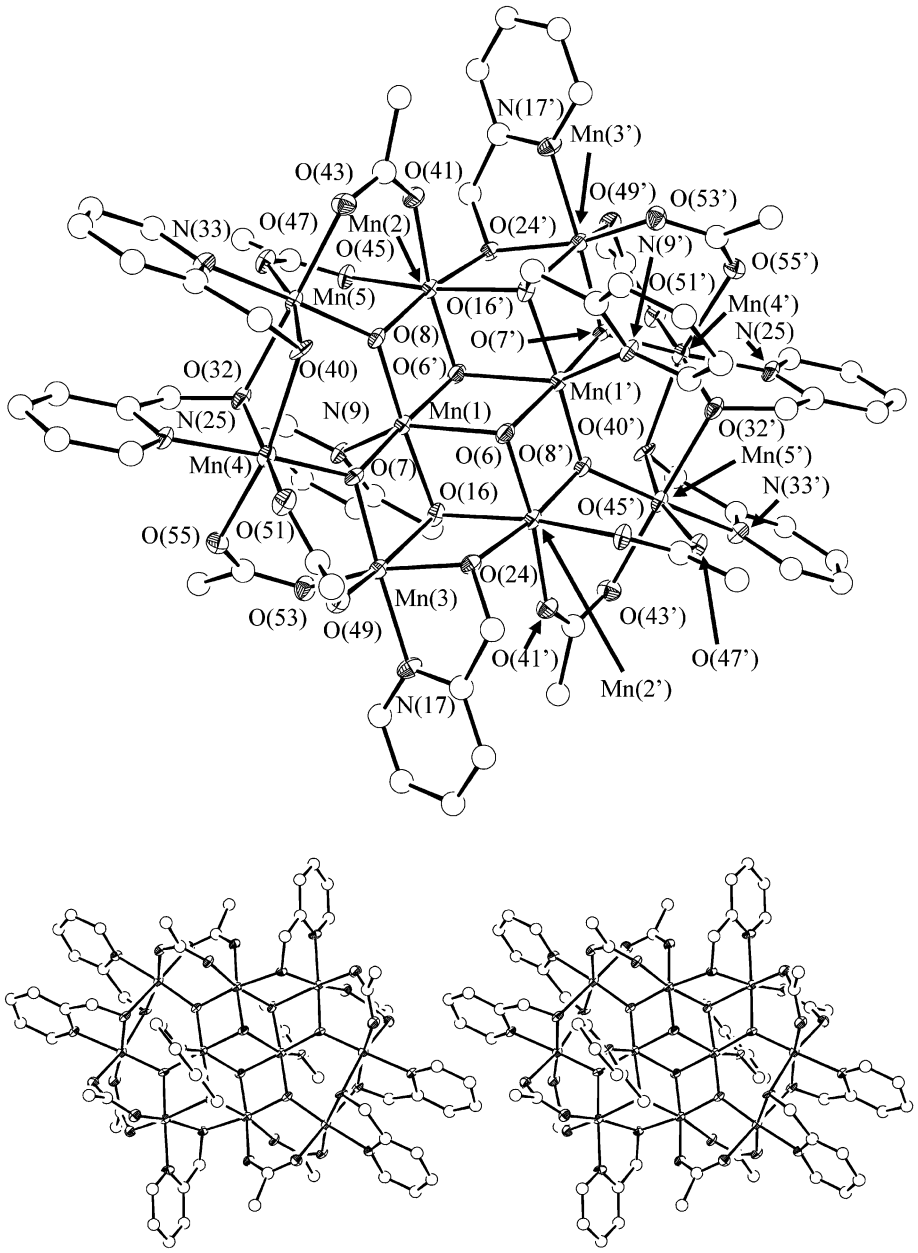

Figure 1. ORTEP representation and stereopair of the centrosymmetric cation of complex **1** at the 50% probability level. Hydrogen atoms have been omitted for clarity.

present work, even though the oxidation level is very different, because it contains a similar central Mn_6 unit with an overall layered structure. Again, the ground state has not been reported.[19]

Complex **2** was obtained from the comproportionation reaction between $MnCl_2$ and $NBu^n{}_4MnO_4$, in a 3:2 ratio in the presence of hmpH. This ratio on paper gives an average Mn oxidation state in solution of Mn^{IV}, but again, the solution likely contains a complicated mixture. Complex **2** ($4Mn^{II}$, $3Mn^{III}$) was isolated from this solution in 30% yield. In an attempt to increase the yield of the product, the Mn^{II}/MnO_4^- ratio was increased to that which would give an average of +2.4, as found in **2**, but this resulted in no formation of this product.

The reaction was performed in the presence of $NBu^n{}_4ClO_4$ to afford the ClO_4^- salt of this Mn_7 cation. We had previously isolated the same cation but as the mixed cation and anion salt $(NEt_4)[Mn_7(OH)_3(hmp)_9Cl_3](Cl)(MnCl_4)$, which was reported in the preliminary communication of this work.[20] However, the presence of the paramagnetic $[MnCl_4]^{2-}$ counterion was undesirable in the magnetic characterization of the Mn_7 species, and so the ClO_4^- salt was targeted and successfully prepared.

A few other Mn_7 complexes have also been reported previously. The reaction between $MnCl_2$, NaOMe, dibenzoylmethane (dbmH), and oxygen in anhydrous MeOH was found to yield $[Mn_7(OMe)_{12}(dbm)_6]$.[21] This complex contains $Mn^{II}{}_3Mn^{III}{}_4$ and possesses an $S = {}^{17}/_2$ ground state. The

(19) Hagen, K. S.; Armstrong, W. H.; Olmstead, M. M. *J. Am. Chem. Soc.* **1989**, *111*, 774.

(20) Bolcar, M. A.; Aubin, S. M. J.; Folting, K.; Hendrickson, D. N.; Christou, G. *J. Chem. Soc., Chem. Commun.* **1997**, 1485.

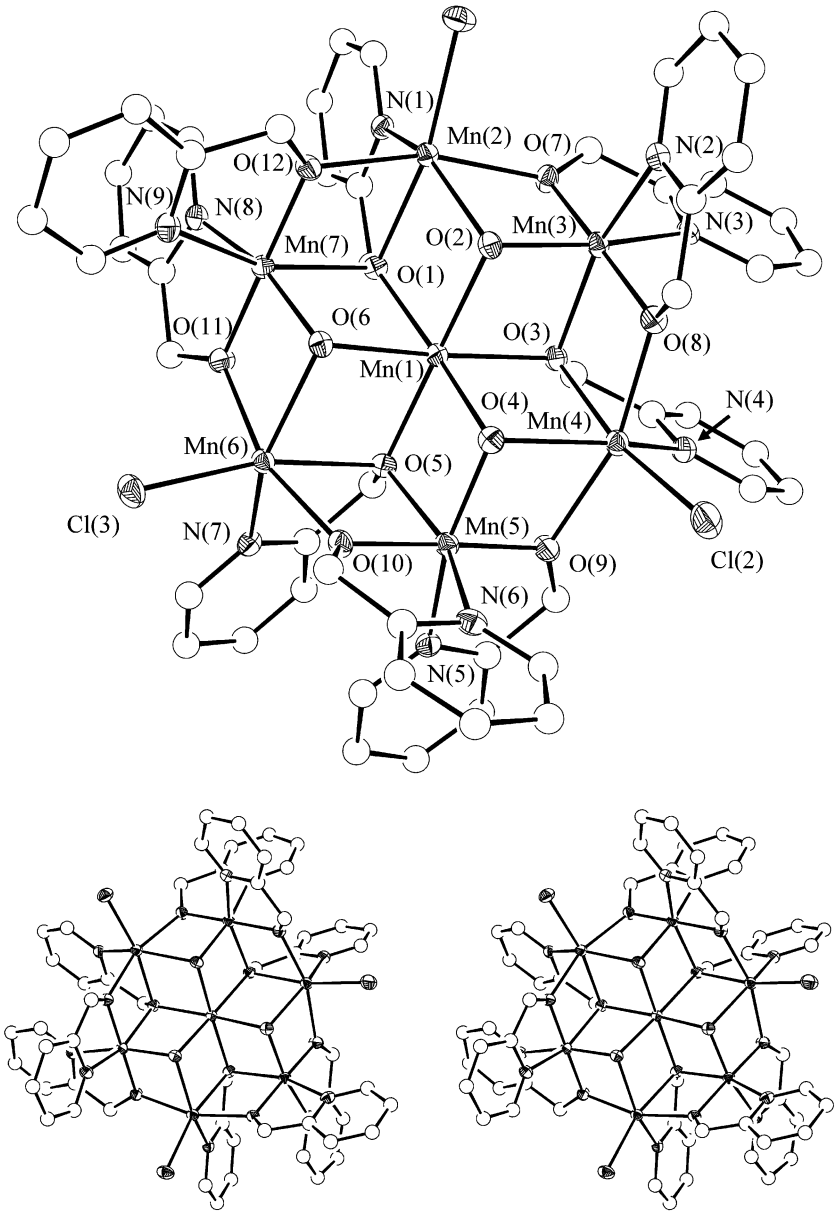

Figure 2. ORTEP representation and stereopair of the cation of complex **2** at the 50% probability level. Hydrogen atoms have been omitted for clarity.

complex $[Mn_7(teaH)_3(tea)_3](ClO_4)_2$ ($teaH_3$ is triethanolamine)[22] contains a $Mn^{II}_4Mn^{III}_3$ core very similar to that of **2**, with an essentially identical Mn_7 topology. Magnetic susceptibility measurements concluded that the ground state is $S = 11$. Finally, the complex $(NEt_4)[Mn_7O_4(O_2CMe)_{10}(dbm)_4]$ has an extended Mn_7 topology and an $S = 4$ ground state.[23a]

The Mn_{10} and Mn_7 nuclearities of **1** and **2** may be put into context by noting that the largest molecular Mn cluster currently known is $[Mn_{30}O_{24}(OH)_8(O_2CCH_2Bu^t)_{32}(H_2O)_2(MeNO_2)_4]$,[23b] followed by $[Mn_{26}O_{16}(OH)_{10}(OMe)_6F_{10}(bta)_2(btaH)_2(MeOH)_{13}(H_2O)]$, where btaH is benzotriazole.[23c]

Description of Crystal Structures. Labeled ORTEP[24] plots of complexes **1** and **2** are presented in Figures 1 and 2, respectively. Selected bond lengths and angles are listed in Tables 2 and 3, respectively.

Complex $\mathbf{1}\cdot 2py\cdot 10CH_2Cl_2\cdot 2H_2O$ crystallizes in the triclinic space group $P\bar{1}$ with the Mn_{10} cation lying on a crystallographic center of symmetry. The cation consists of 10 Mn^{III} ions, 4 μ_3-O^{2-} ions, 2 μ_3-OH^- ions, 8 bridging acetate groups, and 8 bridging hmp^- ligands. There are two types of hmp^- ligands: six containing μ_2-O atoms and two containing μ_3-O atoms, involving O(16) and O(16′). All Mn atoms are six-coordinate and experience a Jahn−Teller axial distortion (elongation), as expected for a high-spin d^4 ion in near-

(21) Abbati, G. L.; Cornia, A.; Fabretti, A. C.; Caneschi, A.; Gatteschi, D. *Inorg. Chem.* **1998**, *37*, 3759.
(22) Pilawa, B.; Kelemen, M. T.; Wanka, S.; Giesselmann, A.; Barra, A. L. *Europhys. Lett.* **1998**, *43*, 7.
(23) (a) Wang, S.; Tsai, H. L.; Streib, W. E.; Christou, G.; Hendrickson, D. N. *J. Chem. Soc., Chem. Commun.* **1992**, 677. (b) Soler, M.; Rumberger, E.; Folting, K.; Hendrickson, D. N.; Christou, G. *Polyhedron* **2001**, *20*, 1365. (c) Jones, L. F.; Brechin, E. K.; Collison, D.; Harrison, A.; Teat, S. J.; Wernsdorfer, W. *Chem. Commun.* **2002**, 2974.
(24) (a) Johnson, C. K.; Burnett, M. N. *ORTEP-III*; Report ORNL-6895; Oak Ridge National Laboratory: Oak Ridge, TN, 1996. (b) Farrugia, L. J. *J. Appl. Crystallogr.* **1997**, *30*, 565.

Table 2. Selected Distances (Å) and Angles (deg) for Complex **1**

Mn(1)−O(6′)	1.875(6)	Mn(3)−O(49)	2.155(7)
Mn(1)−O(6)	2.314(6)	Mn(3)−O(53)	1.920(6)
Mn(1)−O(7)	1.921(6)	Mn(3)−N(17)	2.030(8)
Mn(1)−O(8)	1.892(6)	Mn(4)−O(7)	1.882(6)
Mn(1)−O(16)	1.987(6)	Mn(4)−O(32)	1.883(7)
Mn(1)−N(9)	2.297(8)	Mn(4)−O(40)	2.276(6)
Mn(2)−O(6′)	1.873(6)	Mn(4)−O(51)	1.914(7)
Mn(2)−O(8)	1.885(6)	Mn(4)−O(55)	2.233(7)
Mn(2)−O(16′)	2.205(6)	Mn(4)−N(25)	2.044(8)
Mn(2)−O(24′)	1.982(6)	Mn(5)−O(8)	1.869(6)
Mn(2)−O(41)	1.958(6)	Mn(5)−O(32)	2.238(7)
Mn(2)−O(45)	2.173(6)	Mn(5)−O(40)	1.898(6)
Mn(3)−O(7)	1.880(6)	Mn(5)−O(43)	2.178(7)
Mn(3)−O(16)	2.253(6)	Mn(5)−O(47)	1.940(6)
Mn(3)−O(24)	1.956(6)	Mn(5)−N(33)	2.042(8)

O(6′)−Mn(1)−O(6)	81.12(26)	O(7)−Mn(4)−O(32)	94.39(27)
O(6)−Mn(1)−O(7)	91.86(25)	O(7)−Mn(4)−O(40)	94.38(25)
O(6′)−Mn(1)−O(7)	172.4(3)	O(7)−Mn(4)−O(51)	94.98(28)
O(6)−Mn(1)−O(8)	97.07(25)	O(7)−Mn(4)−O(55)	91.85(26)
O(6′)−Mn(1)−O(8)	82.64(27)	O(7)−Mn(4)−N(25)	172.7(3)
O(6)−Mn(1)−O(16)	78.14(24)	O(32)−Mn(4)−O(40)	80.11(25)
O(6′)−Mn(1)−O(16)	97.50(26)	O(32)−Mn(4)−O(51)	167.5(3)
O(6)−Mn(1)−N(9)	149.49(25)	O(32)−Mn(4)−O(55)	88.14(27)
O(6′)−Mn(1)−N(9)	88.82(28)	O(32)−Mn(4)−N(25)	81.8(3)
O(7)−Mn(1)−O(8)	95.47(27)	O(40)−Mn(4)−O(51)	90.88(26)
O(7)−Mn(1)−O(16)	83.76(26)	O(40)−Mn(4)−O(55)	167.08(24)
O(7)−Mn(1)−N(9)	98.7(3)	O(40)−Mn(4)−N(25)	91.05(28)
O(8)−Mn(1)−O(16)	175.11(27)	O(51)−Mn(4)−O(55)	99.9(3)
O(8)−Mn(1)−N(9)	110.18(27)	O(51)−Mn(4)−N(25)	89.8(3)
O(16)−Mn(1)−N(9)	74.71(26)	O(55)−Mn(4)−N(25)	81.9(3)
O(6′)−Mn(2)−O(8)	82.88(27)	O(8)−Mn(5)−O(32)	89.12(25)
O(6′)−Mn(2)−O(16′)	83.36(26)	O(8)−Mn(5)−O(40)	91.51(27)
O(6′)−Mn(2)−O(24′)	88.95(26)	O(8)−Mn(5)−O(43)	92.49(26)
O(6′)−Mn(2)−O(41)	171.4(3)	O(8)−Mn(5)−O(47)	97.56(27)
O(6′)−Mn(2)−O(45)	99.03(26)	O(8)−Mn(5)−N(33)	173.3(3)
O(8)−Mn(2)−O(16′)	97.49(25)	O(32)−Mn(5)−O(40)	80.82(26)
O(8)−Mn(2)−O(24′)	171.68(27)	O(32)−Mn(5)−O(43)	177.91(24)
O(8)−Mn(2)−O(41)	98.73(27)	O(32)−Mn(5)−O(47)	89.13(26)
O(8)−Mn(2)−O(45)	92.08(26)	O(32)−Mn(5)−N(33)	90.7(3)
O(16′)−Mn(2)−O(24′)	79.89(24)	O(40)−Mn(5)−O(43)	97.80(27)
O(16′)−Mn(2)−O(41)	88.10(26)	O(40)−Mn(5)−O(47)	166.4(3)
O(16′)−Mn(2)−O(45)	170.36(24)	O(40)−Mn(5)−N(33)	81.88(28)
O(24′)−Mn(2)−O(41)	89.11(26)	O(43)−Mn(5)−O(47)	91.98(27)
O(24′)−Mn(2)−O(45)	90.79(25)	O(43)−Mn(5)−N(33)	87.5(3)
O(41)−Mn(2)−O(45)	89.33(26)	O(47)−Mn(5)−N(33)	89.1(3)
O(7)−Mn(3)−O(16)	77.72(25)	Mn(1)−O(6)−Mn(1′)	98.88(26)
O(7)−Mn(3)−O(24)	96.39(27)	Mn(1)−O(6)−Mn(2′)	99.12(27)
O(7)−Mn(3)−O(49)	91.21(27)	Mn(1′)−O(6)−Mn(2′)	97.7(3)
O(7)−Mn(3)−O(53)	95.8(3)	Mn(1)−O(7)−Mn(3)	106.7(3)
O(7)−Mn(3)−N(17)	175.9(3)	Mn(1)−O(7)−Mn(4)	127.6(3)
O(16)−Mn(3)−O(24)	79.24(24)	Mn(3)−O(7)−Mn(4)	118.9(3)
O(16)−Mn(3)−O(49)	161.74(25)	Mn(1)−O(8)−Mn(2)	96.7(3)
O(16)−Mn(3)−O(53)	91.94(26)	Mn(1)−O(8)−Mn(5)	134.0(4)
O(16)−Mn(3)−N(17)	102.9(3)	Mn(2)−O(8)−Mn(5)	119.8(3)
O(24)−Mn(3)−O(49)	87.75(25)	Mn(1)−O(16)−Mn(2′)	99.38(27)
O(24)−Mn(3)−O(53)	163.03(27)	Mn(1)−O(16)−Mn(3)	91.76(24)
O(24)−Mn(3)−N(17)	79.8(3)	Mn(2′)−O(16)−Mn(3)	91.91(23)
O(49)−Mn(3)−O(53)	103.72(28)	Mn(2′)−O(24)−Mn(3)	108.9(3)
O(49)−Mn(3)−N(17)	87.1(3)	Mn(4)−O(32)−Mn(5)	99.10(27)
O(53)−Mn(3)−N(17)	88.2(3)	Mn(4)−O(40)−Mn(5)	97.35(26)

octahedral geometry. The Mn^{III} oxidation states were confirmed by bond valence sum calculations.[25] The two OH^- oxygen atoms are assigned as O(6) and O(6′), based on the bond valence sum calculations[26] and also on the presence of an O−H···N hydrogen-bonding contact with the pyridine molecules of crystallization in the lattice (O···N = 2.614 Å).

The $[Mn_{10}O_4(OH)_2(O_2CMe)_8]^{4+}$ core is relatively planar, with the inner core of six Mn atoms (Mn(1), Mn(1′), Mn(2), Mn(2′), Mn(3), and Mn(3′)) almost perfectly so (Figure 3, top). This inner unit can be described as four face-sharing Mn_3O_4 partial cubane (i.e., cuboidal) units. The side view in Figure 3 also emphasizes that the core is composed of alternating layers of O, Mn, and O atoms. This is similar to the Mn and O arrangements in the AX_2 layered structures of the minerals lithiophorite (Al, Li)$MnO_2(OH)_2$[27] and chalcophonite, $ZnMn_3O_7\cdot 3H_2O$.[28] This type of layered structure has also been seen in the cluster $[Mn_{21}O_{24}(OMe)_8(O_2CCH_2{}^tBu)_{16}(H_2O)_{11}]$, composed of $Mn^{III}{}_9Mn^{IV}{}_{12}$.[29]

It is interesting that the μ_3-OH^- ions bridge very asymmetrically. Thus, Mn(1)−O(6′) and Mn(2)−O(6′) are 1.873(6) and 1.875(6) Å, respectively, whereas Mn(1)−O(6) is much longer at 2.314(6)Å. This is the result of O(6) lying on the Jahn−Teller (JT) elongation axis of Mn(1). Similarly, the alkoxide O atom O(16) of the triply bridging hmp^- group also bridges asymmetrically as a result of it lying on the JT elongation axes of both Mn(2) and Mn(3). Bond lengths to these Mn atoms are 2.205(6) and 2.253(6) Å, respectively, whereas Mn(1)−O(16) is 1.987(6) Å. As a result of the JT-elongated bonds Mn(1)−O(6), Mn(2)−O(16′), and their symmetry-related partners all being parallel, the inner, planar Mn6 core of **1** can reasonably be described as two linear and planar $[Mn(\mu\text{-}O)_2Mn(\mu\text{-}O)_2Mn]$ units held together by the above JT-elongated bonds; these two linear units contain Mn(1), Mn(2), Mn(3) and Mn(1′), Mn(2′), Mn(3′). The linear $[Mn_3O_4]$ is commonly encountered as a recognizable subfragment of higher nuclearity Mn clusters, such as Mn_{11}[30] and Mn_{18},[8] but has never been isolated as a discrete unit in a trinuclear system.

Complex $\mathbf{2}\cdot 3CH_2Cl_2\cdot H_2O$ crystallizes in the triclinic space group $P\bar{1}$ with the Mn_7 cation in a general position. The cation consists of six Mn atoms arranged in a ring around a central, seventh Mn atom. The Mn atoms are held together by three μ_3-OH^- ions and nine bridging and chelating hmp^- ligands. Peripheral ligation is completed by three terminal chloride ions. Six of the hmp^- ligands contain μ_2-O atoms, and three contain μ_3-O atoms, the latter comprising atoms O(1), O(3), and O(5), which together with the μ_3-OH^- ions, O(2), O(4), and O(6), hold in place the central Mn(1) atom. All the Mn atoms are six-coordinate and possess near-octahedral geometry. On the basis of bond valence sum calculations and the identification of the Jahn−Teller distortions expected for Mn^{III} ions, the Mn_7 cation was determined to be mixed-valent $4Mn^{II}$, $3Mn^{III}$. Atoms Mn(1), Mn(2), Mn(4), and Mn(6) are the Mn^{II} ions, and Mn(3), Mn(5), and Mn(7) are the Mn^{III} ions. In addition, atoms O(2), O(4), and O(6) were identified as part of the OH^- ions by bond valence sum calculations and the presence of hydrogen-bonding contacts to the chloride anion Cl(4), which is closely associated with the complex (Figure 3, bottom). The distances from Cl(4) to these hydroxide O atoms O(2), O(4), and O(6) are 3.176(3), 3.160(3), and 3.214(3) Å, respectively, which are values typical of O−H···Cl hydrogen bonds. The

(25) Brown, I. D.; Altermatt, D. *Acta Crystallogr., Sect. B.* **1985**, *41*, 244.
(26) Zhang, X.-Y.; O'Connor, C. J.; Jameson, G. B.; Pope, M. T. *Inorg. Chem.* **1996**, *35*, 30.
(27) Wadsley, A. D. *Acta Crystallogr.* **1952**, *5*, 676.
(28) Wadsley, A. D. *Acta Crystallogr.* **1955** *8*, 165.
(29) Brockman, J. T.; Huffman, J. C.; Christou, G. *Angew. Chem., Int. Ed.* **2002**, *41*, 2506.
(30) Perlepes, S. P.; Huffman, J. C.; Christou, G. *J. Chem. Soc., Chem. Commun.* **1991**, 1657.

Table 3. Selected Distances (Å) and Angles (deg) for Complex **2**

Mn(1)−O(5)	2.131(2)	Mn(3)−N(3)	2.061(3)	Mn(6)−O(10)	2.165(2)
Mn(1)−O(3)	2.141(2)	Mn(3)−O(3)	2.229(2)	Mn(6)−O(11)	2.186(2)
Mn(1)−O(1)	2.143(2)	Mn(3)−N(2)	2.243(3)	Mn(6)−O(6)	2.229(2)
Mn(1)−O(2)	2.221(2)	Mn(4)−O(8)	2.172(2)	Mn(6)−N(7)	2.234(3)
Mn(1)−O(4)	2.230(2)	Mn(4)−O(9)	2.192(2)	Mn(6)−O(5)	2.279(2)
Mn(1)−O(6)	2.235(2)	Mn(4)−O(4)	2.209(2)	Mn(6)−Cl(3)	2.3957(10)
Mn(2)−O(12)	2.164(2)	Mn(4)−N(4)	2.229(3)	Mn(7)−O(11)	1.867(2)
Mn(2)−O(7)	2.192(2)	Mn(4)−O(3)	2.268(2)	Mn(7)−O(12)	1.880(2)
Mn(2)−O(2)	2.222(2)	Mn(4)−Cl(2)	2.4141(11)	Mn(7)−O(6)	1.948(2)
Mn(2)−N(1)	2.239(3)	Mn(5)−O(9)	1.860(2)	Mn(7)−N(8)	2.063(3)
Mn(2)−O(1)	2.254(2)	Mn(5)−O(10)	1.888(2)	Mn(7)−O(1)	2.228(2)
Mn(2)−Cl(1)	2.4047(10)	Mn(5)−O(4)	1.948(3)	Mn(7)−N(9)	2.242(3)
Mn(3)−O(7)	1.865(2)	Mn(5)−N(5)	2.072(3)	Cl(4)···O(2)	3.176(3)
Mn(3)−O(8)	1.891(2)	Mn(5)−O(5)	2.220(2)	Cl(4)···O(4)	3.160(3)
Mn(3)−O(2)	1.947(2)	Mn(5)−N(6)	2.236(3)	Cl(4)···O(6)	3.214(3)

O(6′)−Mn(1)−O(6)	81.12(26)	O(32)−Mn(4)−O(40)	80.11(25)	N(8)−Mn(7)−O(1)	94.48(9)
O(6)−Mn(1)−O(7)	91.86(25)	O(32)−Mn(4)−O(51)	167.5(3)	O(11)−Mn(7)−N(9)	104.84(10)
O(6′)−Mn(1)−O(7)	172.4(3)	O(32)−Mn(4)−O(55)	88.14(27)	O(12)−Mn(7)−N(9)	78.78(10)
O(6)−Mn(1)−O(8)	97.07(25)	O(32)−Mn(4)−N(25)	81.8(3)	O(6)−Mn(7)−N(9)	95.24(10)
O(6′)−Mn(1)−O(8)	82.64(27)	O(40)−Mn(4)−O(51)	90.88(26)	N(8)−Mn(7)−N(9)	91.07(10)
O(6)−Mn(1)−O(16)	78.14(24)	O(40)−Mn(4)−O(55)	167.08(24)	O(1)−Mn(7)−N(9)	159.37(9)
O(6′)−Mn(1)−O(16)	97.50(26)	O(40)−Mn(4)−N(25)	91.05(28)	Mn(1)−O(6)−Mn(1′)	98.88(26)
O(6)−Mn(1)−N(9)	149.49(25)	O(51)−Mn(4)−O(55)	99.9(3)	Mn(1)−O(6)−Mn(2′)	99.12(27)
O(6′)−Mn(1)−N(9)	88.82(28)	O(51)−Mn(4)−N(25)	89.8(3)	Mn(1′)−O(6)−Mn(2′)	97.7(3)
O(7)−Mn(1)−O(8)	95.47(27)	O(55)−Mn(4)−N(25)	81.9(3)	Mn(1)−O(7)−Mn(3)	106.7(3)
O(7)−Mn(1)−O(16)	83.76(26)	O(8)−Mn(5)−O(32)	89.12(25)	Mn(1)−O(7)−Mn(4)	127.6(3)
O(7)−Mn(1)−N(9)	98.7(3)	O(8)−Mn(5)−O(40)	91.51(27)	Mn(3)−O(7)−Mn(4)	118.9(3)
O(8)−Mn(1)−O(16)	175.11(27)	O(8)−Mn(5)−O(43)	92.49(26)	Mn(1)−O(8)−Mn(2)	96.7(3)
O(8)−Mn(1)−N(9)	110.18(27)	O(8)−Mn(5)−O(47)	97.56(27)	Mn(1)−O(8)−Mn(5)	134.0(4)
O(16)−Mn(1)−N(9)	74.71(26)	O(8)−Mn(5)−N(33)	173.3(3)	Mn(2)−O(8)−Mn(5)	119.8(3)
O(6′)−Mn(2)−O(8)	82.88(27)	O(32)−Mn(5)−O(40)	80.82(26)	Mn(1)−O(16)−Mn(2′)	99.38(27)
O(6′)−Mn(2)−O(16′)	83.36(26)	O(32)−Mn(5)−O(43)	177.91(24)	Mn(1)−O(16)−Mn(3)	91.76(24)
O(6′)−Mn(2)−O(24′)	88.95(26)	O(32)−Mn(5)−O(47)	89.13(26)	Mn(1)−O(16)−C(15)	117.0(5)
O(6′)−Mn(2)−O(41)	171.4(3)	O(32)−Mn(5)−N(33)	90.7(3)	Mn(2′)−O(16)−Mn(3)	91.91(23)
O(6′)−Mn(2)−O(45)	99.03(26)	O(40)−Mn(5)−O(43)	97.80(27)	Mn(2′)−O(16)−C(15)	122.9(5)
O(8)−Mn(2)−O(16′)	97.49(25)	O(40)−Mn(5)−O(47)	166.4(3)	Mn(3)−O(16)−C(15)	126.6(6)
O(8)−Mn(2)−O(24′)	171.68(27)	O(40)−Mn(5)−N(33)	81.88(28)	Mn(2′)−O(24)−Mn(3)	108.9(3)
O(8)−Mn(2)−O(41)	98.73(27)	O(43)−Mn(5)−O(47)	91.98(27)	Mn(2′)−O(24)−C(23)	118.8(5)
O(8)−Mn(2)−O(45)	92.08(26)	O(43)−Mn(5)−N(33)	87.5(3)	Mn(3)−O(24)−C(23)	112.2(5)
O(16′)−Mn(2)−O(24′)	79.89(24)	O(47)−Mn(5)−N(33)	89.1(3)	Mn(4)−O(32)−Mn(5)	99.10(27)
O(16′)−Mn(2)−O(41)	88.10(26)	O(10)−Mn(6)−O(11)	162.54(9)	Mn(4)−O(32)−C(31)	113.7(6)
O(16′)−Mn(2)−O(45)	170.36(24)	O(10)−Mn(6)−O(6)	95.48(9)	Mn(5)−O(32)−C(31)	119.8(5)
O(24′)−Mn(2)−O(41)	89.11(26)	O(11)−Mn(6)−O(6)	69.96(9)	Mn(4)−O(40)−Mn(5)	97.35(26)
O(24′)−Mn(2)−O(45)	90.79(25)	O(10)−Mn(6)−N(7)	96.34(9)	Mn(4)−O(40)−C(39)	117.0(5)
O(41)−Mn(2)−O(45)	89.33(26)	O(11)−Mn(6)−N(7)	91.17(9)	Mn(5)−O(40)−C(39)	114.5(5)
O(7)−Mn(3)−O(16)	77.72(25)	O(6)−Mn(6)−N(7)	145.51(10)	Mn(2)−O(41)−C(42)	134.3(6)
O(7)−Mn(3)−O(24)	96.39(27)	O(10)−Mn(6)−O(5)	74.71(8)	Mn(5)−O(43)−C(42)	124.1(6)
O(7)−Mn(3)−O(49)	91.21(27)	O(11)−Mn(6)−O(5)	92.61(8)	Mn(2)−O(45)−C(46)	124.5(6)
O(7)−Mn(3)−O(53)	95.8(3)	O(6)−Mn(6)−O(5)	79.24(8)	Mn(5)−O(47)−C(46)	135.6(6)
O(7)−Mn(3)−N(17)	175.9(3)	N(7)−Mn(6)−O(5)	72.88(9)	Mn(3)−O(49)−C(50)	129.0(6)
O(16)−Mn(3)−O(24)	79.24(24)	O(10)−Mn(6)−Cl(3)	97.83(6)	Mn(4)−O(51)−C(50)	127.3(6)
O(16)−Mn(3)−O(49)	161.74(25)	O(11)−Mn(6)−Cl(3)	96.78(6)	Mn(3)−O(53)−C(54)	126.2(6)
O(16)−Mn(3)−O(53)	91.94(26)	O(6)−Mn(6)−Cl(3)	112.73(7)	Mn(4)−O(55)−C(54)	125.1(6)
O(16)−Mn(3)−N(17)	102.9(3)	N(7)−Mn(6)−Cl(3)	97.56(8)	Mn(1)−N(9)−C(10)	131.7(6)
O(24)−Mn(3)−O(49)	87.75(25)	O(5)−Mn(6)−Cl(3)	166.78(6)	Mn(1)−N(9)−C(14)	109.5(6)
O(24)−Mn(3)−O(53)	163.03(27)	O(11)−Mn(7)−O(12)	175.23(10)	Mn(3)−N(17)−C(18)	127.2(7)
O(24)−Mn(3)−N(17)	79.8(3)	O(11)−Mn(7)−O(6)	83.11(10)	Mn(3)−N(17)−C(22)	113.2(6)
O(49)−Mn(3)−O(53)	103.72(28)	O(12)−Mn(7)−O(6)	99.76(10)	Mn(4)−N(25)−C(26)	127.8(7)
O(49)−Mn(3)−N(17)	87.1(3)	O(11)−Mn(7)−N(8)	81.06(11)	Mn(4)−N(25)−C(30)	111.9(6)
O(53)−Mn(3)−N(17)	88.2(3)	O(12)−Mn(7)−N(8)	95.88(11)	Mn(5)−N(33)−C(34)	127.1(6)
O(7)−Mn(4)−O(32)	94.39(27)	O(6)−Mn(7)−N(8)	164.00(11)	Mn(5)−N(33)−C(38)	113.7(6)
O(7)− Mn(4)−O(40)	94.38(25)	O(11)−Mn(7)−O(1)	95.64(9)	O(2)···Cl(4)···O(4)	60.41(6)
O(7)−Mn(4)−O(51)	94.98(28)	O(12)−Mn(7)−O(1)	80.90(9)	O(2)···Cl(4)···O(6)	59.65(6)
O(7)−Mn(4)−O(55)	91.85(26)	O(6)−Mn(7)−O(1)	84.73(9)	O(4)···Cl(4)···O(6)	59.50(6)
O(7)−Mn(4)−N(25)	172.7(3)				

cation has virtual C_3 symmetry. The Jahn−Teller elongation axes at the Mn^{III} ions are N(2)−Mn(3)−O(3), N(6)−Mn(5)−O(5), and N(9)−Mn(7)−O(1), each involving one of the μ_3-O atoms of the hmp^- ligands. The core of complex **2** is also relatively planar, as emphasized in Figure 3, and in analogy with **1** can be described as consisting of six Mn_3O_4 partial cubane units, each doubly face-sharing and all vertex-sharing at the central Mn ion. In addition, complex **2** has an alternating O, Mn, O layered structure (Figure 3, bottom), similar to that in complex **1**.

Magnetic Susceptibility Studies. Solid-state variable-temperature magnetic susceptibility measurements were performed on a vacuum-dried sample of complex **1**·$^1/_2$py, suspended in eicosane to prevent torquing. The dc magnetic

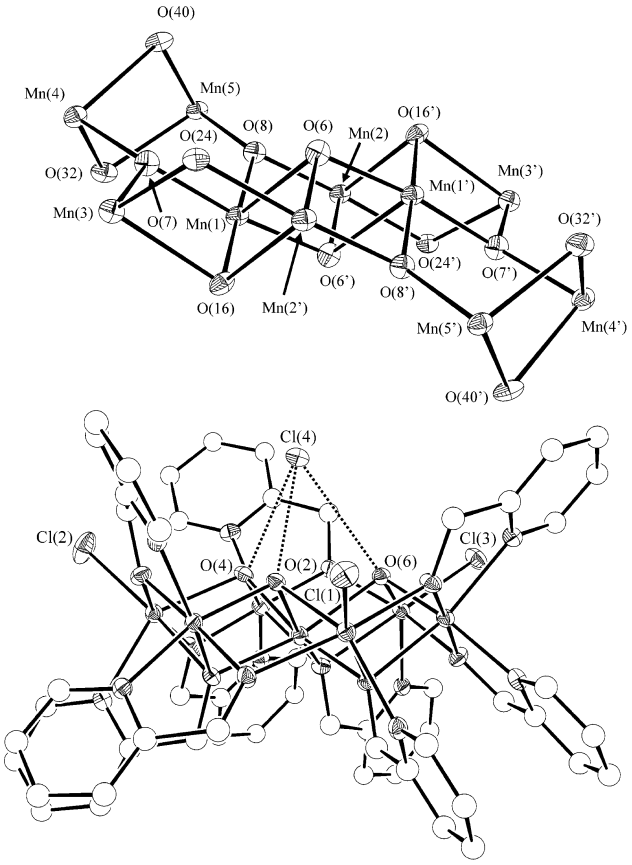

Figure 3. ORTEP representations of the cores of the cations of complexes **1** (top) and **2** (bottom) at the 50% probability level. The views are from the side in order to emphasize the alternating O/Mn/O layered structures of both cations and the O−H···Cl hydrogen bonds (dashed lines) to the chloride anion of the cation of **2**.

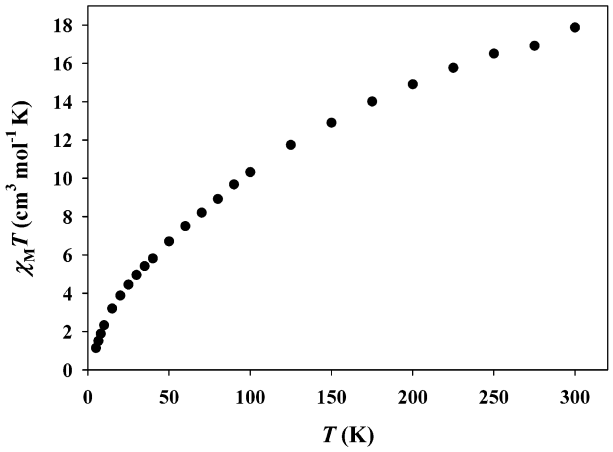

Figure 4. Plot of $\chi_M T$ vs temperature for complex **1**.

susceptibility (χ_M) data were collected in the 5.0−300 K range in a 0.5 T magnetic field (Figure 4). The $\chi_M T$ value gradually decreases from 17.87 cm^3 mol^{-1} K at 300 K to 1.14 cm^3 mol^{-1} K at 5.0 K. The value of $\chi_M T$ at 300 K is much lower than that expected for a cluster of 10 noninteracting Mn^{III} ions (30.00 cm^3 mol^{-1} K for $g = 2$), suggesting the presence of intramolecular antiferromagnetic exchange interactions between the constituent Mn^{III} ions. Because of the topological complexity of the molecule, it is not possible to determine the individual pairwise Mn_2 exchange interac-

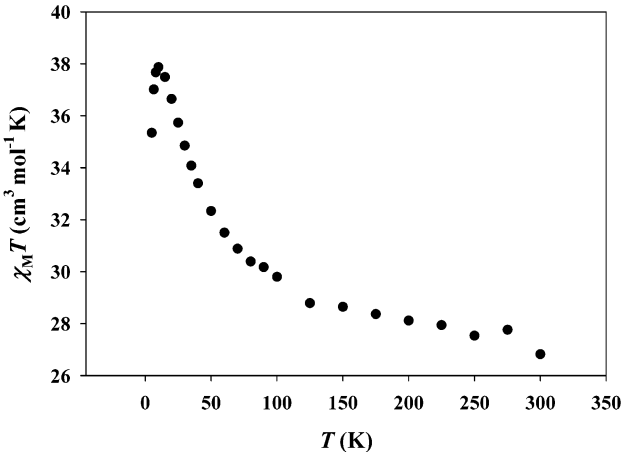

Figure 5. Plot of $\chi_M T$ vs temperature for complex **2**.

tions using the Kambe method,[31] but the experimental data strongly suggest that the cation has a ground-state spin value of $S = 0$.

Similar solid-state variable-temperature magnetic susceptibility measurements were performed on a vacuum-dried sample of complex **2**, suspended in eicosane to prevent torquing. The dc magnetic susceptibility (χ_M) data were collected in the 5.0−300 K range in a 0.5 T magnetic field (Figure 5). The $\chi_M T$ value at 300 K of 26.8 cm^3 mol^{-1} K is essentially the value expected if the constituent $Mn^{II}_4Mn^{III}_3$ ions were noninteracting (26.5 cm^3 mol^{-1} K for $g = 2$), and it increases with decreasing temperature to a maximum of 37.9 cm^3 mol^{-1} K at ∼10 K, before decreasing at lower temperatures. The maximum indicates a relatively large spin ground state (S), and the low-temperature decrease is assigned to a combination of zero-field splitting (ZFS) and intermolecular antiferromagnetic exchange interactions or both. Although complex **2** is smaller than **1**, it is still not possible to apply the Kambe method.

To determine the spin of the ground state, magnetization (M) measurements were performed in the 1.80−4.00 K temperature range and the 0.5−3.0 T dc magnetic field range. The data are plotted as reduced magnetization ($M/(N\mu_B)$) versus H/T in Figure 6, where N is Avogadro's number, μ_B is the Bohr magneton, and H is the applied magnetic field. For a system occupying only the ground state and experiencing no ZFS, the various isofield lines would be superimposed and $M/(N\mu_B)$ would saturate at a value of gS. The nonsuperposition of the isofield lines in Figure 6 is indicative of the presence of significant zero-field splitting. The data were fit using the method described elsewhere[14,32] that involves diagonalization of the spin Hamiltonian matrix, assuming only the ground state is occupied at these temperatures and including axial ZFS ($D\hat{S}_z^2$), Zeeman interactions, and a full powder average of the magnetization. The best and equally good fits to the data are obtained with $S = 10$, $g = 2.13$, $D = -0.14$ cm^{-1} (−0.20 K) and $S = 11$, $g = 1.94$, $D = -0.11$ cm^{-1} (−0.16 K), with the latter fit being slightly preferred because of its reasonable g value. The quality of the fit is reasonable but not as good as normal, and we attribute this

(31) Kambé, K. *J. Phys. Soc. Jpn.* **1950**, *5*, 48.

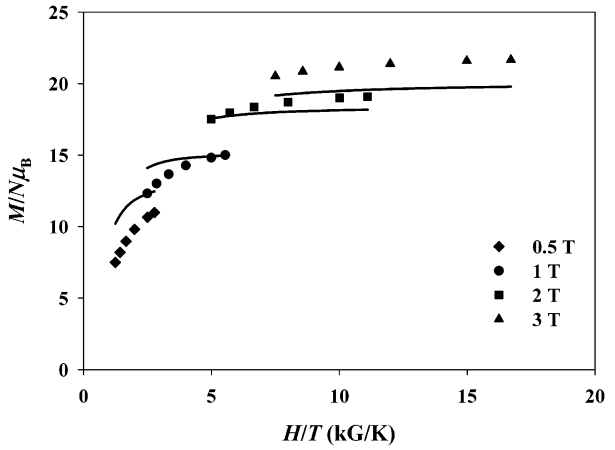

Figure 6. Plot of the reduced magnetization ($M/(N\mu_B)$) vs H/T for complex **2** in the indicated applied fields. The solid lines are the fit of the data; see the text for the fitting parameters.

to the population of low-lying excited states, even at these low temperatures.[33] This is a frequently encountered situation in molecules containing Mn^{II} ions, because exchange interactions involving them are typically very weak (<1 cm^{-1}) and the resulting energy separations are consequently very small. In fact, given the large content of Mn^{II} in complex **2**, it is thus very likely that the ground state is near in energy to *many* other spin states not very far away in energy. We conclude that the Mn_7 cation has an approximately $S = 10$ or 11 ground state but are unable with present data to be any more definitive. Nor can we accurately determine the value of D from these data, given that the indicated values above are only rough estimates because of the less than perfect fits and the fact that axial symmetry is assumed (i.e., the rhombic ZFS parameter E is taken as zero). Similar conclusions regarding the spin ground state were made for $NEt_4[Mn_7(OH)_3Cl_3(hmp)_9](Cl)(MnCl_4)$.[20] $[Mn_7(teaH)_3(tea)_3](ClO_4)_2$, with a similar core to complex **2** and with the same $Mn^{II}_4Mn^{III}_3$ formulation, was concluded from detailed studies to have an $S = 11$ ground state, lending support to our present conclusions about the ground-state spin of **2**.[22]

Hysteresis Measurements below 1.8 K. Complex **2** possesses an $S = 10$ or 11 ground state, and it was thus considered a possibility that it might be a single-molecule magnet (SMM). If this were the case, then it should exhibit slow relaxation (reorientation) of its magnetization vector. One way of detecting this is the appearance of an imaginary (out-of-phase) signal (χ_M'') in the alternating current (ac) magnetic susceptibility. No such signal was observed down to 1.8 K, the operating limit of our SQUID magnetometer, when **1** was subjected to an ac field of 3.5 G oscillating at frequencies up to 1500 Hz. It was still possible that slow magnetization relaxation might be seen at temperatures below 1.8 K, and this was explored with single-crystal studies down to 0.04 K using a micro-SQUID instrument.[13] Figure 7 shows the plots observed in a magnetization versus dc field scan at

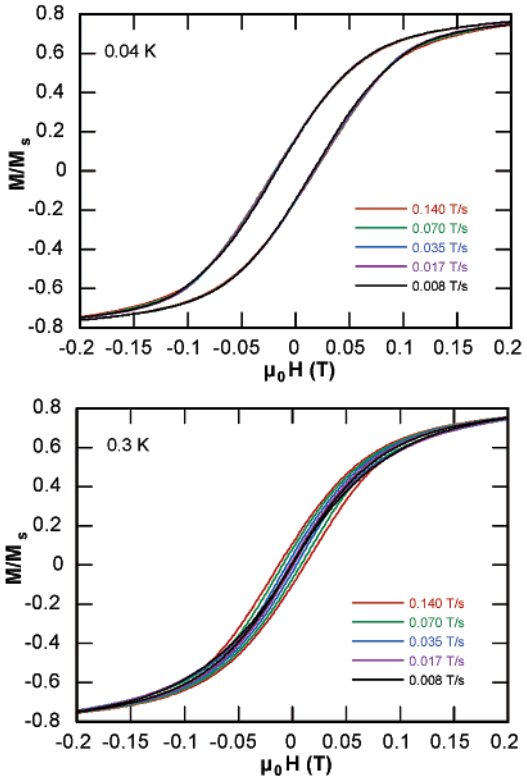

Figure 7. Magnetization (M) vs magnetic field hysteresis loops for complex **2** at the indicated temperatures and sweep rates. M is normalized to its saturation value, M_s.

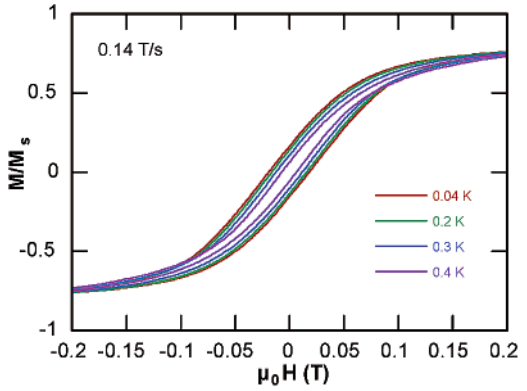

Figure 8. Magnetization (M) vs magnetic field hysteresis loops for complex **2** at a 0.14 T s^{-1} sweep rate and the indicated temperatures. M is normalized to its saturation value, M_s.

0.04 and 0.3 K. A very slight hysteresis behavior was seen, but the coercivity (width) of the loop was independent of the scan rate at 0.04 K and was also essentially so at 0.3 K. This is not the behavior expected from SMMs, which display a marked increase in coercivity with increasing scan rate. Similarly, at a fixed scan rate there was essentially no temperature dependence of the coercivity in a magnetization versus dc field plot (Figure 8). (Note that the field axes in Figures 7 and 8 have been greatly expanded to show what little scan rate or temperature dependence is present.) These results strongly suggest that complex **2** is not a SMM and that the small hysteresis observed at very low temperature is due to intermolecular exchange interactions and long range ordering. The intermolecular interactions need only be very

(32) Yoo, J.; Yamaguchi, A.; Nakano, M.; Krzystek, J.; Streib, W. E.; Brunel, L.-C.; Ishimoto, H.; Christou, G.; Hendrickson, D. N. *Inorg. Chem.* **2001**, *40*, 4604.
(33) Soler, M.; Artus, P.; Folting, K.; Huffman, J. C.; Hendrickson, D. N.; Christou, G. *Inorg. Chem.* **2001**, *40*, 4902.

weak and likely have their origin from both dipolar and exchange contributions.

The absence of a significant barrier to magnetization relaxation for a species with such a large ground-state S value suggests that the ZFS parameter D is very small. The upper limit of the energy barrier to relaxation is $S^2|D|$, and it is likely, therefore, that $|D| < 0.1$ cm^{-1} and perhaps significantly less. In fact, the previously reported complex $[Mn_7(teaH)_3(tea)_3]^{2+}$ mentioned above,[22] which has a similar Mn_7 core to that in **2**, has been shown by EPR measurements to have $D = -0.08$ cm^{-1} and a rhombic zero-field splitting parameter, $E = -2.1 \times 10^{-4}$ cm^{-1}. Such a correspondingly small D value is likely also for **2** and is actually consistent with the structure of this cation. The main sources of the molecular anisotropy are the three JT distorted Mn^{III} ions. The projections of the these single-ion anisotropies onto the molecular anisotropy axis will determine the value of the molecular D parameter. As described above, the three Mn^{III} JT elongation axes are the N(2)−Mn(3)−O(3), N(6)−Mn(5)−O(5), and N(9)−Mn(7)−O(1) axes (Figure 2), which are disposed in a propeller-like fashion and lie almost in the Mn_7 plane. Thus, the projections of these onto the molecular easy axis (z axis) will give a very small net molecular axial anisotropy, D. In any case, as already mentioned, the value $S^2|D|$ merely represents the upper limit (U) to the energy barrier, with the true (or effective) barrier (U_{eff}) to magnetization relaxation being significantly less because of quantum tunneling of the magnetization through the barrier via higher energy M_S levels of the ground S state.

Conclusions

Decanuclear complex **1** has been obtained from the reaction of $[Mn_3O(O_2CMe)_6(py)_3](ClO_4)$ with hmpH and possesses an $S = 0$ ground state. In contrast, the comproportionation reaction between $MnCl_2 \cdot 4H_2O$ and $NBu^n_4MnO_4$ in the presence of hmpH yields heptanuclear complex **2**, which has an $S = 10$ or 11 ground state. The dramatic difference in ground-state spin values for complexes with not too dissimilar nuclearities and ligation emphasizes the difficulty in trying to deliberately synthesize complexes with large spin values. In addition, the described results also emphasize that in the search for new SMMs, obtaining a large spin value is not enough: $S \geq 10$ is one of the largest spin values ever obtained for a molecular cluster, but in the absence also of a significant anisotropy, as reflected in the ZFS parameter D, the magnetization relaxation is fast, and the molecule is not an SMM. Nevertheless, other areas of Mn cluster chemistry continue to provide new examples of SMMs, and the number of known examples continues to grow.

Acknowledgment. This work was supported by the National Science Foundation.

Supporting Information Available: X-ray crystallographic files in CIF format for complexes **1**·2py·10CH_2Cl_2·2H_2O and **2**·3CH_2Cl_2·H_2O. This material is available free of charge via the Internet at http://pubs.acs.org.

IC0348906